International Journal of Engineering Science 49 (2011) 839–855

Contents lists available at ScienceDirect

International Journal of Engineering Science

journal homepage: www.elsevier.com/locate/ijengsci

Nonlinear elastic mechanics of the ball-loaded blister test

MingHao Zhao [a,b,*], WeiLing Zheng [b], CuiYing Fan [a], Ernian Pan [a,c]

[a] The School of Mechanical Engineering, Zhengzhou University, Zhengzhou, Henan 450001, China
[b] Department of Engineering Mechanics, Zhengzhou University, Zhengzhou, Henan 450001, China
[c] Department of Civil Engineering, University of Akron, OH 44325, USA

ARTICLE INFO

Article history:
Received 23 January 2011
Accepted 22 April 2011
Available online 31 May 2011

Keywords:
Blister test
Thin film
Compliant substrate
Contact
Deflection–load relation

ABSTRACT

The nonlinear elastic mechanics of spherically capped shaft or ball-loaded blister tests is presented. In the test model, a thin film is attached to a substrate with a circular hole running through the thickness of the substrate. A central load is applied to the film through the hole by a spherically capped shaft or a ball with a finite radius. The deformed blister is divided into two parts: a circular region in contact with the sphere of the cap or ball and an outer noncontact annulus. The Reissner's plate theory is employed to describe the deformation of the contact part and the von Kármán plate theory for the noncontact annulus. A constitutive equation of coupled linear springs is obtained to quantify the effect of the substrate deformation on the blister deflection. For small deflection, the analytical solution of load-deflection is derived. For large deflection, an iteration approach is adopted to predict numerically the load-deflection curve. Finite-element analysis is conducted to verify the analytical and numerical solutions. The influence of the substrate deformation, residual stress, radius of the spherical cap or ball and the friction between the film and ball on the load–deflection relation is investigated.

1. Introduction

Thin film structures have been widely used in micro/nano-electronic mechanical systems (MEMS/NEMS). The reliability and life span of MEMS/NEMS depend strongly on the mechanical properties e.g., elastic modulus, residual stress and adhesion property. Thus, testing and characterizing the mechanical property of the thin-film/substrate systems are important, and as such, a number of test methods have been developed. These include the peel and pull-off (Gecit, 1987; Gent & Hamed, 1977), scratch (Perry, 1983; Volinsky, Moody, & Gerberich, 2002), indentation (Antunes, Fernandes, Sakharova, Oliveira, & Menezes, 2007; Lee, Barber, & Thouless, 2009), nanoindentation (Li & Chou, 1997; Pharr & Oliver, 1992), four-point bending (Lee, Huang, Chang, & Wang, 2009), microcantilever (Kahrobaiyan, Asghari, Rahaeifard, & Ahmadian, 2010; Weihs, Hong, Bravman, & Nix, 1988), microbridge (Zhang, Su, Qian, Zhao, & Chen, 2000) and bulge/blister (Dannenberg, 1961; Williams, 1969) methods. Among these methods, the bulge/blister test is particularly important and so is the mechanics of the blister test.

The first blister test was proposed by Dannenberg (1961) to measure the adhesion of thick organic coatings on metals. Later, Williams (1969) introduced the pressurized circular blister test to measure adhesive fracture energy. Bennett, Devries, and Williams (1974) studied the adhesive fracture mechanics where the finite-element analysis (FEA) was used, along with experiment for verifying the basic analysis. Hinkley (1983) tested the adhesion of polymer films to the oxidized silicon substrate. Voorthuyzen and Bergveld (1984) obtained the blister deflection–pressure curves by considering both the bending and tensile stresses based on the von Kármán plate equation. Small and Nix (1992) reviewed the existing models on the

* Corresponding author at: The School of Mechanical Engineering, Zhengzhou University, No. 100 Science Road, Zhengzhou, Henan Province 450001, China. Tel.: +86 371 67781752; fax: +86 371 67781786.

E-mail addresses: memhzhao@zzu.edu.cn, memhzhao@sina.com (M. Zhao).

0020-7225/$ - see front matter © 2011 Elsevier Ltd. All rights reserved.
doi:10.1016/j.ijengsci.2011.04.007

deformation behavior of a circular thin film in a bulge test, analyzed these models via FEA, and proposed a procedure along with a set of equations for analyzing the bulge test data in order to secure the reliability and improve the accuracy of this technique. Chang and Peng (1992) conducted a nonlinear elastic analysis of a blister test for the rubber-like material described by the Ogden–Tschoegl strain energy function. The dependence of the specific adhesive fracture energy on the critical pressure was analyzed for a blister test specimen with different geometry and different material constants. Sizemore, Hohlfelder, Vlassak, and Nix (1995) discussed the blister test mechanics and proposed a simple equation relating adhesion to the height of the blister and the pressure on the blister. Using this relation, the adhesion energies of diamond thin films to silicon substrates were extracted from the experimental data. Using the blister test, Khan (1995) analyzed biaxial stretching for the simulation of fractures in composites. Hohlfelder, Luo, Vlasska, Chidsey, and Nix (1997) summarized the derivation of the crack extension force for the blister test. They discussed how blister tests could be conducted by measuring only the pressure and volume of the liquid injected into the test system, and based on this, described a way to calculate the velocity of the interface crack front. Hbaieb and Zhang (2005) conducted an FEA simulation of a blister test of an elastic–plastic film bonded to a substrate under plane-strain deformation. A traction–separation law was used to model the fracture process ahead of the crack tip at the interface between the thin film and substrate. They also suggested a method to extract the adhesion energy and the interface strength. Arjun and Wan (2005) derived the strain energy release rate from first principles and showed that the gradual change in blister profile over the entire loading process must be considered in order to calculate correctly the strain energy release rate. Jiang, Zhou, Liao, and Sun (2008) conducted a geometrically nonlinear FEA study of a blister test where an elastic–plastic film was bonded to an elastic–plastic substrate. The fracture process ahead of the crack tip at the interface between the thin film and substrate was described by a built-in cohesive model.

In the original blister tests, the delamination or debonding is caused by the gas or liquid pressure. The disadvantages of this type of blister test are that: (1) the energy release rate increases with the radius of the debonding, which is unstable and could lead to catastrophic damage, and (2) such tests may be invalid because of dissolved gases (Lai & Dillard, 1994; Wan, 1999). Therefore, many variant forms of blister test were developed, such as the island blister (Allen & Senturia, 1989), inverted blister (Fernando & Kinloch, 1990), and peninsula blister (Dillard & Bao, 1991) tests. A controlled spherically capped shaft or ball for the displacement or loading was introduced, which is termed as the shaft- or ball-loaded blister test and it is a good alternative to the pressurized test (Malyshev & Salganik, 1965; O'Brien, Ward, Guo, & Dillard, 2003). The shaft-loaded blister test was first proposed by Malyshev and Salganik (1965) for the fracture energy. Wan and Mai (1995) developed an analytical solution for the strain energy release rate of thin flexible membranes with conical geometry, and presented further an analysis of the plastic yielding at the contact area of the shaft tip. Also by employing the shaft-loaded blister, Jin and Wang (2008) obtained the nonlinear deflection of the thin circular membrane, under rigidly clamped and loosely clamped boundary conditions, with and without the residual stress. Based on the nonlinear von Kármán equations, Jensen (1991) analyzed the blister test under either a hydrostatic pressure or a point load, and presented the strain energy release rate and the associated mode mixity. Arbitrary and independent values of the elastic constants of the film and substrate were considered. Later, Jensen and Thouness (1993) studied the effect of the residual stress in the blister test. Jin (2008) theoretically analyzed the energy release rate and bending-to-stretching behavior in the shaft-loaded blister test.

A point load would lead to the stress singularity, and thus, a spherically capped shaft or ball with a finite radius can be used to determine the mechanical properties of the thin flexible membrane (Wan & Liao, 1999). Liao and Wan (2000) used a cylindrical shaft with an attached steel ball to determine the adhesion strength of a film–substrate system under cyclic loading. Using a shaft with a stainless steel ball, Xu, Shearwood, and Liao (2003) measured the film mechanical properties when the film was on a rigid substrate. Kozlova, Braccini, Eustathopoulos, Devismes, and Dupeux (2008) tested the mechanical resistance of metal/ceramic brazing joints with a steel ball in order to avoid the ceramic fracture. Wan, Guo, and Dillard (2003) derived an analytical constitutive relation for the punch-loaded blister based on the von Kármán equations, and further carried out a nonlinear FEA to verify their closed-form solution. Zhao, Zheng, and Fan (2010) derived an analytical solution for the flat-end shaft-loaded blister test.

So far, however, there are still two outstanding issues which are important to the spherically capped shaft- or ball-loaded blister test method. One is the effect of the contact between a bending film and a sphere when loading is applied, and the other is the influence of the substrate deformation, especially for a hard film on a soft substrate. The substrate was assumed to be rigid in previous models. Therefore, motivated by these, we propose to develop, in this paper, the mechanics of spherically capped shaft- or ball-loaded blister tests and derive the load–deflection solution. This paper is organized as follows: In Section 2 we will present the governing equation and the general solution for the noncontact annulus film based on the von Kármán's plate theory. In Section 3, the governing equation and the general solution for the circular contact film are presented on the basis of the Reissner's plate theory, which will avoid the strange zero-force phenomenon in the contact area between a bending film and a rigid cylinder from the classical beam theory (Timoshenko, 1957). The boundary and continuity conditions are presented in Section 4. The final solutions for both small and large deflections are derived in Section 5. The influence of the friction between the film and spherical cap or ball is discussed in Section 6, and conclusions are drawn in Section 7.

2. Governing equations and general solutions for the noncontact area

A thin film of thickness h is attached to a substrate with a circular hole of radius a passing through the substrate as shown in Fig. 1(a). A central load P_0 is applied to the film by a spherically capped shaft or rigid ball of radius R to deflect the film. The

deformed blister is divided into two parts as shown in Fig. 1(b). One is the circular contact region with radius c, and the other is the outer annulus with width a–c. If the load is sufficiently large, delamination or debonding of size Δa is induced as shown in Fig. 1(b).

Because of axial symmetry, a cylindrical coordinate system orz is introduced with the plane $z = 0$ being the middle plane of the film. According to the von Kármán plate theory, the governing equations for the deformation of the noncontact annulus are (Timoshenko & Woinowsky-Krieger, 1959)

$$D\frac{1}{r}\frac{d}{dr}\left\{r\frac{d}{dr}\left[\frac{1}{r}\frac{d}{dr}(r\frac{dw_n}{dr})\right]\right\} - \frac{1}{r}\frac{d}{dr}\left(rN_{rn}\frac{dw_n}{dr}\right) = 0, \quad c \leqslant r \leqslant a, \tag{1}$$

$$r^2\frac{d^2N_{rn}}{dr^2} + 3r\frac{dN_{rn}}{dr} + \frac{E_f h}{2}\left(\frac{dw_n}{dr}\right)^2 = 0, \tag{2}$$

In Eqs. (1) and (2), w_n is the vertical deflection and D is the flexural rigidity given by $D = \frac{E_f h^3}{12(1-\nu_f^2)}$, where E_f and ν_f are, respectively, the elastic modulus and Poisson's ratio of the film, with the subscripts "f" and "n" referring to the film and the "noncontact area". Also in Eq. (1), N_{rn} is the radial force per unit width in the film:

$$N_{rn} = N_0 + \Delta N_{rn}, \quad N_0 = \sigma_0 h, \tag{3}$$

where σ_0 is the residual stress uniformly distributed in the film and ΔN_{rn} is the change in radial force due to the applied force P_0.

In general, it is difficult to obtain the analytical solution to Eqs. (1) and (2). However, in the case of small deflection, $N_{rn} = N_0$ is constant. Then, the general solution to Eq. (1) can be derived in the analytical form (Zhao, Zheng, et al., 2010)

$$W_n(x) = \frac{C_2}{n^2}[-1 + I_0(nx)] + \frac{C_3}{n^2}K_0(nx) + C_4 + C_1\log x, \quad x_0 \leqslant x \leqslant 1, \tag{4}$$

where $I_0(x)$ and $K_0(x)$ are, respectively, the first- and second-kind modified Bessel functions of zero order, and

$$x = r/a, x_0 = c/a, \quad n = \sqrt{N_0 a^2/D}, \quad N_0 > 0, \quad W_n(x) = w_n(r)/h. \tag{5}$$

The constants C_1, C_2, C_3 and C_4 in Eq. (4) will be determined from the boundary and continuity conditions. The bending moment M_n and shear force Q_n in the film are expressed in terms of the deflection:

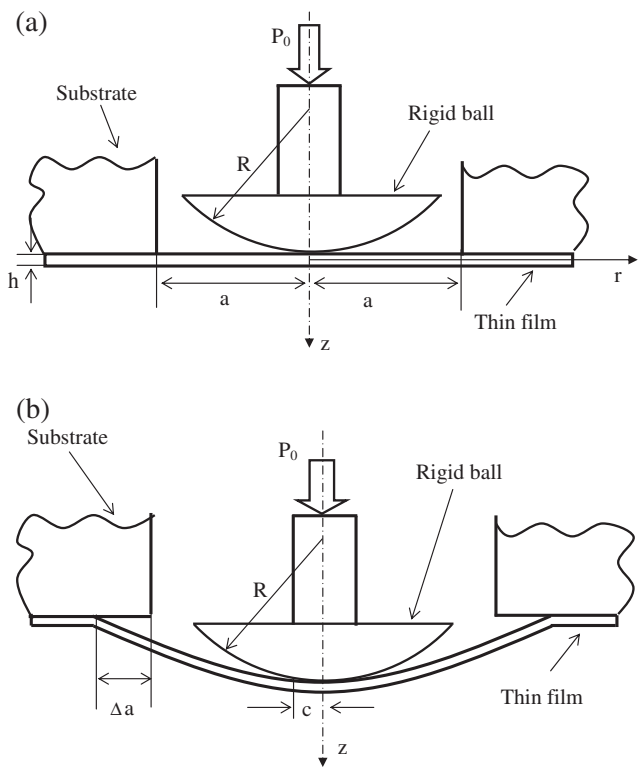

Fig. 1. (a) Spherically capped shaft blister test. (b) Deformation of the blister.

$$M_n = -D\left[\frac{d^2 w_n}{dr^2} + \frac{\nu_f}{r}\frac{dw_n}{dr}\right] = -D\frac{h}{a^2}\left[\frac{d^2 W_n}{dx^2} + \frac{\nu_f}{x}\frac{dW_n}{dx}\right], \tag{6a}$$

$$Q_n = -D\left[\frac{d^3 w_n}{dr^3} + \frac{1}{r}\frac{d^2 w_n}{dr^2} - \frac{1}{r^2}\frac{dw_n}{dr}\right] = -D\frac{h}{a^3}\left[\frac{d^3 W_n}{dx^3} + \frac{1}{x}\frac{d^2 W_n}{dx^2} - \frac{1}{x^2}\frac{dW_n}{dx}\right], \tag{6b}$$

while the radial displacement u_n of the middle plane of the film can be expressed in terms of the change in radial force:

$$u_n = \frac{r}{E_f h}\left[r\frac{d\Delta N_{rn}}{dr} + (1-\nu_f)\Delta N_{rn}\right]. \tag{6c}$$

3. Governing equations and general solutions for the circular contact film

In the study of the contact between a beam and a rigid cylinder, Timoshenko (1957) found a strange phenomenon, that is, there was no contact force in the contact area if the classical beam theory was used. The reason for this phenomenon is that the shear deformation is restricted in the classical beam theory. Thus, he proposed a high-order beam theory to solve this problem. Mathematically, we find that the governing equations and boundary conditions cannot be matched properly if the classical von Kármán plate theory is employed to the ball-loaded blister deflection analysis. As shown by Timoshenko (1957) and Johnson (1985), it is necessary to use a higher-order plate theory to study the contact between a ball and the bending film. Reddy and Wang (2000) analyzed the difference among the classical plate, first-order shear deformation (or Reissner's plate), and the third-order shear deformation theories, and demonstrated the effect of the shear deformation on the classical solutions. Comparing these higher-order theories, Ma and Wang (2004) and Zhao, Zhang, and Zhang (2010) observed that the Reissner's plate theory is accurate for the shear deformation in axially symmetric circular plates. Therefore, we employ the Reissner's plate theory to describe the deformation of the inner circular contact film.

Assuming that there is no friction in the contact area, the nonlinear governing equations for large deflection are then given by (Zhao, Zhang, et al., 2010)

$$D\left(\frac{\partial^2\phi_c}{\partial r^2} + \frac{1}{r}\frac{\partial\phi_c}{\partial r} - \frac{1}{r^2}\phi_c\right) + C\left(\frac{\partial w_c}{\partial r} - \phi_c\right) = 0, \tag{7a}$$

$$C\left(\frac{\partial^2 w_c}{\partial r^2} + \frac{1}{r}\frac{\partial w_c}{\partial r} - \frac{\partial\phi_c}{\partial r} - \frac{1}{r}\phi_c\right) + N_{rc}\frac{\partial^2 w_c}{\partial r^2} + \frac{\partial w_c}{\partial r}\frac{\partial N_{rc}}{\partial r} + \frac{N_{rc}}{r}\frac{\partial w_c}{\partial r} = 0, \tag{7b}$$

$$\frac{\partial^2 u_c}{\partial r^2} + \frac{1}{r}\frac{\partial u_c}{\partial r} - \frac{u_c}{r^2} + \frac{\partial w_c}{\partial r}\frac{\partial^2 w_c}{\partial r^2} + \frac{1-\nu_f}{2r}\left(\frac{\partial w_c}{\partial r}\right)^2 = 0, \tag{7c}$$

where u_c and w_c are the displacements of the middle plane in the r-direction and z-direction, respectively, ϕ_c denotes the rotation of the normal of the middle plane, and $C = \frac{5E_f h}{12(1+\nu_f)}$ is the shearing rigidity, with subscript "c" referring to the "contact area". The change in the resultant force ΔN_{rc} can be expressed in terms of the displacement:

$$\Delta N_{rc} = \frac{E_f h}{1-\nu_f^2}\left[\frac{\partial u_c}{\partial r} + \nu_f\frac{u_c}{r} + \frac{1}{2}\left(\frac{\partial w_c}{\partial r}\right)^2\right], \tag{8}$$

where $N_{rc} = N_0 + \Delta N_{rc}$.

Since the ball is assumed to be rigid, the deflection can be expressed by

$$w_c = w_{c0} - R\left(1 - \sqrt{1-(r/R)^2}\right), \quad 0 \leqslant r \leqslant c, \tag{9}$$

where w_{c0} is the deflection of the origin point o.

Substituting Eq. (9) into Eq. (7a), we obtain

$$\frac{\partial^2\phi_c}{\partial r^2} + \frac{1}{r}\frac{\partial\phi_c}{\partial r} - \left(\frac{1}{r^2} + \frac{C}{D}\right)\phi_c = \frac{C}{D}\frac{r}{R\sqrt{1-(r/R)^2}}, \quad 0 \leqslant r \leqslant c. \tag{10}$$

Introducing $\varphi_c = \frac{a}{h}\phi_c$, Eq. (10) can be rewritten as

$$\frac{\partial^2\varphi_c}{\partial x^2} + \frac{1}{x}\frac{\partial\varphi_c}{\partial x} - \left(\frac{1}{x^2} + \frac{Ca^2}{D}\right)\varphi_c = \frac{Ca^2}{D}\frac{1}{t}\frac{a}{R}\frac{x}{\sqrt{1-(xa/R)^2}}. \tag{11}$$

Solving Eq. (11) gives

$$\varphi_c = C_5 I_1(bx) + C_6 K_1(bx) + \varphi_{c0}, \tag{12}$$

where $I_1(x)$ and $K_1(x)$ are respectively the first- and second-kind modified Bessel functions of the first order, and

$$b^2 = Ca^2/D, \quad t = h/a, \tag{13}$$

Also in Eq. (12), φ_{c0} is the particular solution of Eq. (11) and is given in Appendix A.

Using the dimensionless parameters in Eq. (5), Eq. (9) can be normalized as

$$W_c = W_{c0} - \frac{R}{h}\left(1 - \sqrt{1 - \left(\frac{xa}{R}\right)^2}\right), \quad 0 \leqslant x \leqslant x_0, \tag{14}$$

where $W_{c0} = w_c(0)/h$, $W_c(x) = w_c(r)/h$, and W_{c0}, C_5, C_6 and x_0 are determined from the boundary and continuity conditions. It should be pointed out that the above solution is valid for large deflection of the plate.

The bending moment and shear force in the film are expressed in terms of the deflection and rotation according to the Reissner's plate theory:

$$M_c = -D\left(\frac{\partial \phi_c}{\partial r} + \nu_f \frac{\phi_c}{r}\right) = -D\frac{h}{a^2}\left(\frac{\partial \varphi_c}{\partial x} + \nu_f \frac{\varphi_c}{x}\right), \tag{15a}$$

$$Q_c = C\left(\frac{\partial w_c}{\partial r} - \phi_c\right) = C\frac{h}{a}\left(\frac{\partial W_c}{\partial x} - \varphi_c\right), \tag{15b}$$

$$\Delta N_{rc} = \frac{E_f h}{1 - \nu_f^2}\left[\frac{\partial u_c}{\partial r} + \nu_f \frac{u_c}{r} + \frac{1}{2}\left(\frac{\partial w_c}{\partial r}\right)^2\right]. \tag{15c}$$

4. Boundary and continuity conditions

4.1. Boundary conditions along the blister edge

Under an applied loading, the substrate deforms along with the film deflection. The inverse effect of the substrate deformation on the deflection of the film can be modeled by the coupled linear springs (Zhang et al., 2000; Zhao, Zhou, Yang, Liu, & Zhang, 2007). Thus, the boundary conditions along the edge of the blister are the continuation of the rotation, deflection and displacement and the balance of the moment, shear force and membrane force:

$$\theta_n = -\theta_s, \quad w_n = -w_s, \quad u_n = -u_s, \tag{16a}$$

$$M_n = -M_s, \quad \Delta N_{rn}\theta_n + Q_n = Q_s, \quad \Delta N_{rn} = \Delta N_s, \quad r = a. \tag{16b}$$

The constitutive equations of the equivalent linear springs are

$$\begin{bmatrix} u_s \\ w_s \\ \theta_s \end{bmatrix} = \begin{bmatrix} S_{NN} & S_{NQ} & S_{NM} \\ S_{QN} & S_{QQ} & S_{QM} \\ S_{MN} & S_{MQ} & S_{MM} \end{bmatrix} \begin{bmatrix} N_s \\ Q_s \\ M_s \end{bmatrix}, \tag{17}$$

where $[S]$ is the generalized compliance matrix, which depends on the properties and geometric parameters of the film and the substrate including Young's modulus and Poisson's ratio E_f, E_s, ν_f and ν_s, as well as on the blister radius thickness ratio a/h. The compliance coefficients can be expressed in terms of their dimensionless counterparts:

$$\begin{aligned} &S_{NN} = \frac{C_{NN}}{\overline{E}_f}, \quad S_{NQ} = \frac{C_{NQ}}{\overline{E}_f} = \frac{C_{QN}}{\overline{E}_f} = S_{QN}, \quad S_{NM} = \frac{C_{NM}}{\overline{E}_f h} = \frac{C_{MN}}{\overline{E}_f h} = S_{MN}, \\ &S_{QQ} = \frac{C_{QQ}}{\overline{E}_f}, \quad S_{MQ} = \frac{C_{MQ}}{\overline{E}_f h} = \frac{C_{QM}}{\overline{E}_f h} = S_{QM}, \quad S_{MM} = \frac{C_{MM}}{\overline{E}_f h^2}, \end{aligned} \tag{18}$$

which are functions of a/h and the Dundur's parameters, which are defined as

$$\alpha = \frac{\overline{E}_f - \overline{E}_s}{\overline{E}_f + \overline{E}_s}, \quad \beta = \frac{1}{2}\frac{\overline{E}_f(1-\nu_f)(1-2\nu_s) - \overline{E}_s(1-2\nu_f)(1-\nu_s)}{\overline{E}_f(1-\nu_f)(1-2\nu_s) + \overline{E}_s(1-2\nu_f)(1-\nu_s)}, \tag{19}$$

where

$$\overline{E}_f = \frac{E_f}{1-\nu_f^2}, \quad \overline{E}_s = \frac{E_s}{1-\nu_s^2}. \tag{20}$$

Since the influence of parameter β is negligible compared with that of α (Zhao et al., 2007), we have set $\beta = 0$ in this paper. All the compliance coefficients are obtained using the FEA as discussed in Zhao et al. (2007), but a hole through the substrate is considered in this paper. The FEA model is shown in Fig. 2(a) and (b). The results demonstrate that neglecting the influence of the hole results in an error of 75% in the compliances. Fitting the FEA results, we obtain the compliant coefficients:

$$\begin{aligned} C_{NN} &= \frac{c_{11}}{c_{12}t+1}, \quad C_{NM} = C_{MN} = \frac{c_{21}}{c_{22}t+1}, \\ C_{NQ} &= C_{QN} = -\frac{c_{31}}{c_{32}t+1}, \quad C_{QQ} = \frac{c_{41}t+1}{c_{42}t+c_{43}}, \\ C_{QM} &= C_{MQ} = \frac{c_{51}t+1}{c_{52}t+c_{53}}, \quad C_{MM} = c_6, \end{aligned} \tag{21}$$

where the parameters c_{ij} depend only on the Dundurs parameter α and are given as

$$c_{11} = 8.4828\frac{(1+\alpha)^{0.4786}}{(1-\alpha)^{0.8355}}, \quad c_{12} = 7.7936\frac{(1+\alpha)^{0.1337}}{(1-\alpha)^{0.8183}}, \tag{22a}$$

$$c_{21} = 0.9122\frac{(1+\alpha)^{0.2174}}{(1-\alpha)^{0.1208}}, \quad c_{22} = 1.4553\frac{(1+\alpha)^{1.0343}}{(1-\alpha)^{0.5040}}, \tag{22b}$$

$$c_{31} = 5.0093\frac{(1+\alpha)^{0.0870}}{(1-\alpha)^{1.0379}}, \quad c_{32} = 8.0657\frac{(1+\alpha)^{-0.2271}}{(1-\alpha)^{0.9997}}, \tag{22c}$$

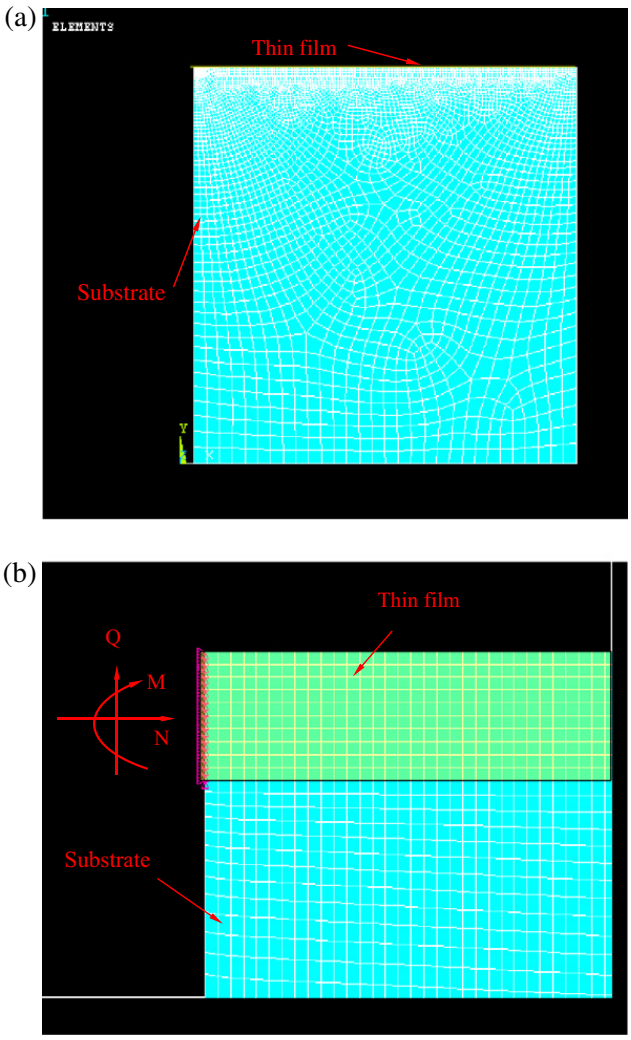

Fig. 2. Typical finite-element mesh for the calculation of the spring compliance: (a) global mesh and (b) local mesh near the hole edge.

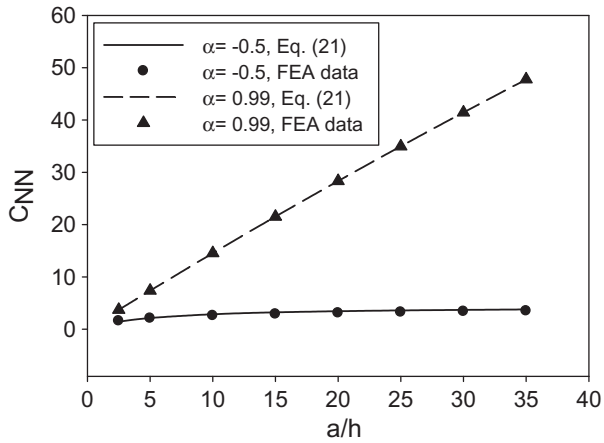

Fig. 3a. Compliance C_{NN}.

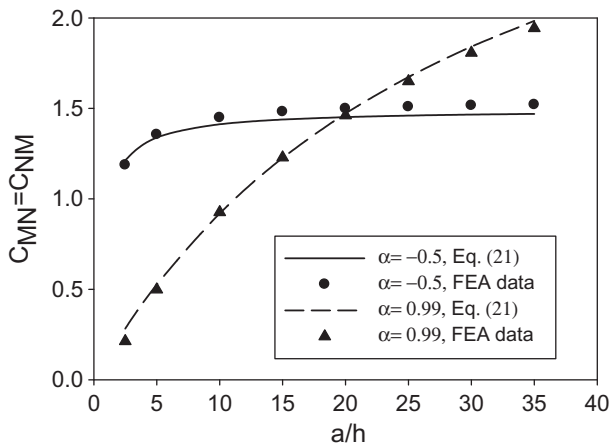

Fig. 3b. Compliance C_{MN}.

$$c_{41} = 3.0038\frac{(1+\alpha)^{0.1561}}{(1-\alpha)^{-0.2895}}, \quad c_{42} = 0.9059\frac{(1+\alpha)^{-0.6989}}{(1-\alpha)^{-0.9034}},$$

$$c_{43} = 0.0854\frac{(1+\alpha)^{-0.8454}}{(1-\alpha)^{-0.8988}}, \tag{22d}$$

$$c_{51} = \frac{(1+\alpha)^{0.6308}}{(1-\alpha)^{0.1474}}(-0.0041 + 0.6372\alpha - 0.9438\alpha^2),$$

$$c_{52} = -0.3498\frac{(1+\alpha)^{0.2924}}{(1-\alpha)^{-1.1672}}, \quad c_{53} = -0.4371\frac{(1+\alpha)^{-0.9892}}{(1-\alpha)^{-0.6972}}, \tag{22e}$$

$$c_6 = 7.2171\frac{(1+\alpha)^{0.3176}}{(1-\alpha)^{0.3559}}. \tag{22f}$$

Fig. 3 shows that the compliances obtained using Eq. (21) fit very well with the FEA data.

From Eqs. (16) and (17), the boundary condition along the blister edge can be rewritten as

$$\begin{aligned} -u_n &= S_{NN}\Delta N_{rn} + S_{NQ}(\Delta N_{rn}\phi_n + Q_n) + S_{NM}M_n, \\ -w_n &= S_{QN}\Delta N_{rn} + S_{QQ}(\Delta N_{rn}\phi_n + Q_n) + S_{QM}M_n, \quad r = a. \\ -\theta_n &= S_{MN}\Delta N_{rn} + S_{MQ}(\Delta N_{rn}\phi_n + Q_n) + S_{MM}M_n. \end{aligned} \tag{23}$$

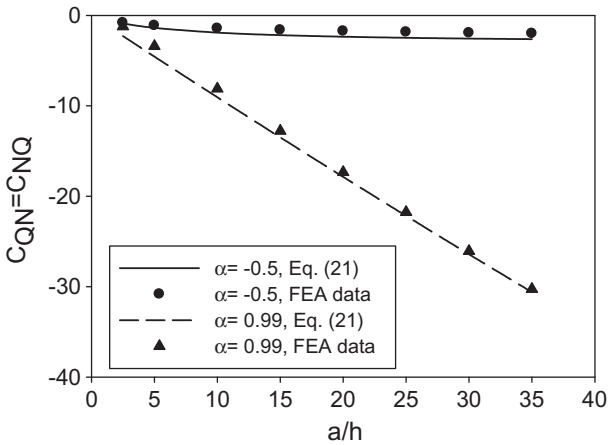

Fig. 3c. Compliance C_{QN}.

At the blister center, we have the condition

$$\begin{aligned} &\phi_c = 0, \\ &u_c = 0, \quad r = 0. \end{aligned} \tag{24}$$

4.2. Continuity conditions along the interface between the contact and noncontact regions

Along the ring interface between the contact and noncontact regions, the solutions for these two regions should satisfy the continuity conditions of the rotation, deflection and displacement, and the balances of the moment, shear force and membrane force:

$$\begin{aligned} &w_c = w_n, \quad \phi_c = \phi_n, \quad u_c = u_n, \\ &M_c = M_n, \quad Q_c = Q_n, \quad \Delta N_{rc} = \Delta N_{rn}, \quad r = c, \\ &\Delta N_{rn}\phi_n + Q_n = -P_0/(2\pi c). \end{aligned} \tag{25}$$

5. Final solutions

5.1. Final solutions in the case of small deflection

Substituting the general solutions in Eqs. (4), (12), and (14) into the boundary and continuity conditions described in the last two subsections gives the following final solutions:

$$W_c = W_{c0} - \frac{R}{h}\left(1 - \sqrt{1 - (xa/R)^2}\right), \quad 0 \leqslant x \leqslant x_0, \tag{26a}$$

$$W_{c0} = \frac{R}{h}\left(1 - \sqrt{1 - (x_0 a/R)^2}\right) + \frac{C_2}{n^2}[-1 + I_0(nx_0)] + \frac{C_3}{n^2}K_0(nx_0) + C_4 + C_1 \log x_0, \tag{26b}$$

$$\varphi_c = C_5 I_1(bx) + C_6 K_1(bx) + \varphi_{c0}, \quad 0 \leqslant x \leqslant x_0, \tag{26c}$$

$$W_n = C_1 \log x + \frac{C_2}{n^2}[-1 + I_0(nx)] + \frac{C_3}{n^2}K_0(nx) + C_4, \quad x_0 \leqslant x \leqslant 1, \tag{26d}$$

where the constants C_i are expressed in terms of x_0 and are given in Appendix B, with x_0 being determined from the following relation

$$\begin{aligned} &\frac{1}{2}bC_5[I_0(bx_0) + I_2(bx_0)] + \left.\frac{\partial \varphi_{c0}}{\partial x}\right|_{x=x_0} + \nu_f \frac{1}{x_0}[C_5 I_1(bx_0) + \varphi_{c0}|_{x=x_0}] \\ &\quad = \frac{C_1}{x_0^2}(\nu_f - 1) + C_2\left[\frac{1}{2}I_0(nx_0) + \frac{\nu_f I_1(nx_0)}{nx_0} + \frac{1}{2}I_2(nx_0)\right] + C_3\left[\frac{1}{2}K_0(nx_0) - \frac{\nu_f K_1(nx_0)}{nx_0} + \frac{1}{2}K_2(nx_0)\right]. \end{aligned} \tag{27}$$

Fig. 4 plots the center deflections of the blister (i.e., the displacement of the loading ball) from both the analytical and FEA results for $R/h = 10$ and $R/h = 100$. The normalized load is given by $P = a^2P_0/(2\pi Dh)$, and other fixed parameters are: $a/h = 15$, $\alpha = 0$, and $n^2 = 0$. In the FEA, axisymmetric PLANE82 elements in ANSYS were used. There are 10 elements in the film

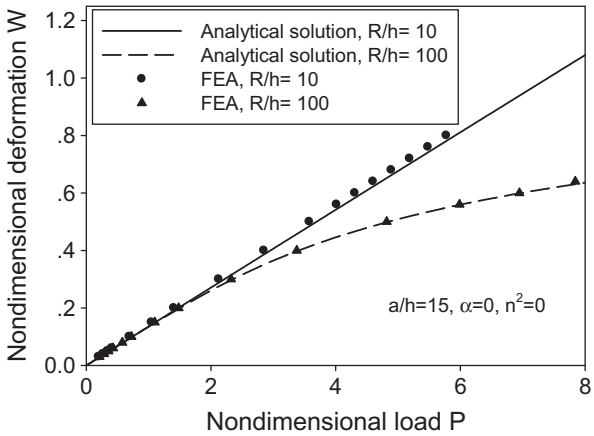

Fig. 4. Comparison of the central deflections between the analytical solution and FEA for $R/h = 10$ and $R/h = 100$ in the case of small deflection.

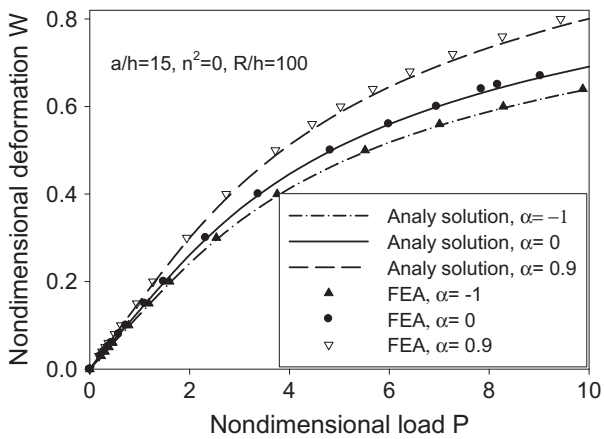

Fig. 5. Comparison of the central deflections between the analytical solution and FEA for different values of Dundur's parameter in the case of small deflection.

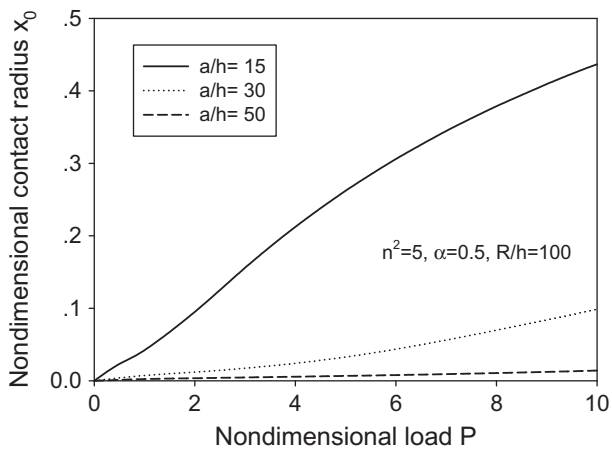

Fig. 6. Influence of the blister radius on the contact radius for fixed $\alpha = 0.5$, $R/h = 100$ and $n^2 = 5$ in the case of small deflection.

thickness direction, and totally about 17,240 elements are used to discretize the film/substrate system. It is observed that the analytical solution agrees well with the FEA result, and that although the deflection is relatively small, the load–deflection relation is not always liner. The nonlinearity of the relation becomes more and more obvious as the ball radius increases.

Fig. 5 plots the dimensionless deflection at the blister center for different Dundur's parameter α but with fixed $a/h = 15$, $n^2 = 0$ and $R/h = 100$. Again, it is observed that the analytical results compare well with those of FEA and that the substrate deformation cannot be ignored. This is particularly true in the case of a hard film on a soft substrate (i.e., $\alpha > 0$).

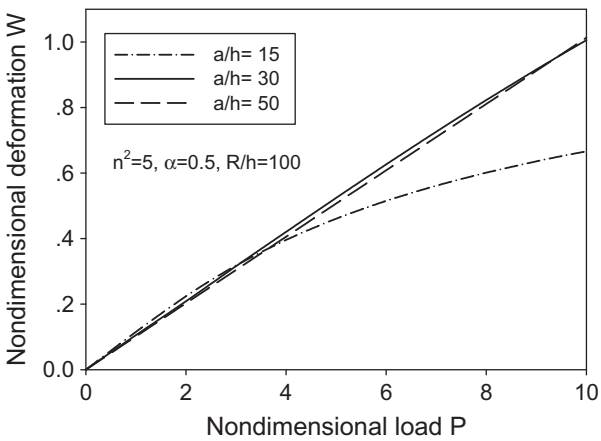

Fig. 7. Influence of the blister radius a/h on the center deflection for $R/h = 100$, $\alpha = 0.5$ and $n^2 = 5$ in the case of small deflection.

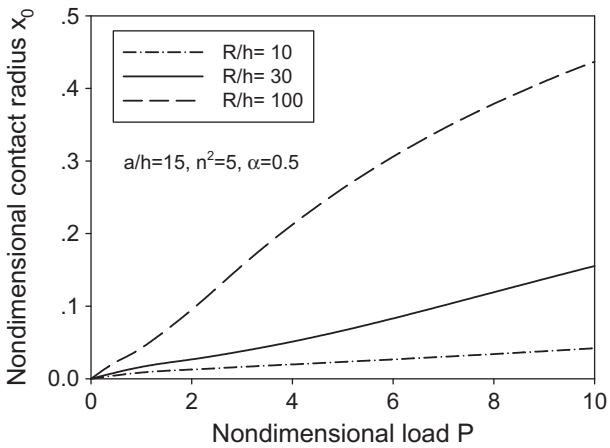

Fig. 8. Influence of the ball radius on the contact radius for $a/h = 15$, $n^2 = 5$ and $\alpha = 0.5$ in the case of small deflection.

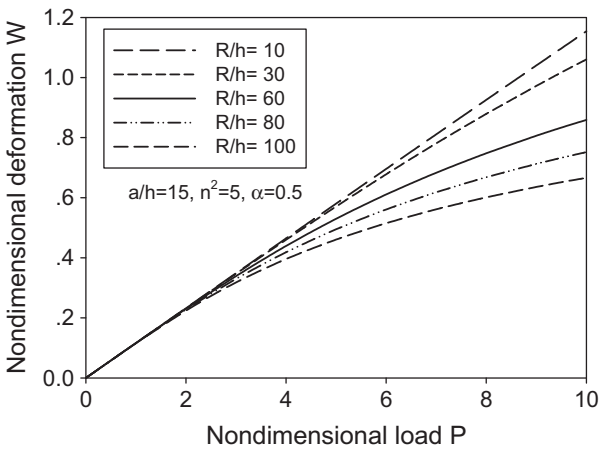

Fig. 9. Influence of the ball radius R/h on the center deflection for $a/h = 15$, $\alpha = 0.5$ and $n^2 = 5$ in the case of small deflection.

The influence of the blister radius a/h on the contact size and on the blister center deflection is, respectively, plotted in Figs. 6 and 7. Other fixed parameters are: $R/h = 100$, $\alpha = 0.5$, and $n^2 = 5$. It is apparent that, for a given load, a large blister size corresponds to a small contact radius (Fig. 6). However, its influence on the deflection–load curve is complicated owing to the contact between the film and spherical cap or ball (Fig. 7).

The radius of the spherical cap or ball (R/h) has a great effect on the contact area and center deflection, as shown, respectively, in Figs. 8 and 9. Other fixed parameters are: $a/h = 15$, $\alpha = 0.5$, and $n^2 = 5$. It is clear that, for a given loading, a large ball radius leads to a large contact radius (Fig. 8) and a small deflection (Fig. 9).

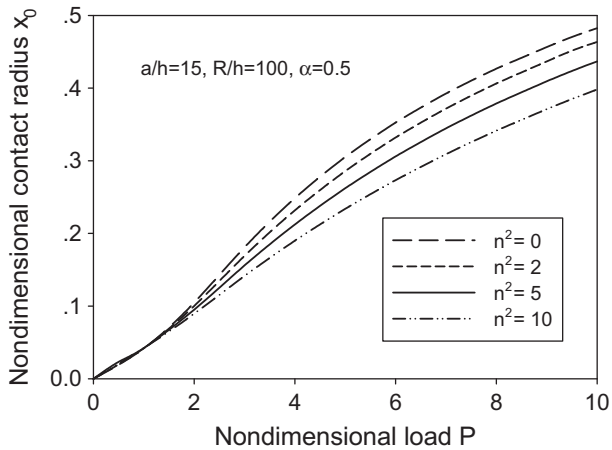

Fig. 10. Influence of residual stress on the contact radius for $a/h = 15$, $R/h = 100$ and $\alpha = 0.5$ in the case of small deflection.

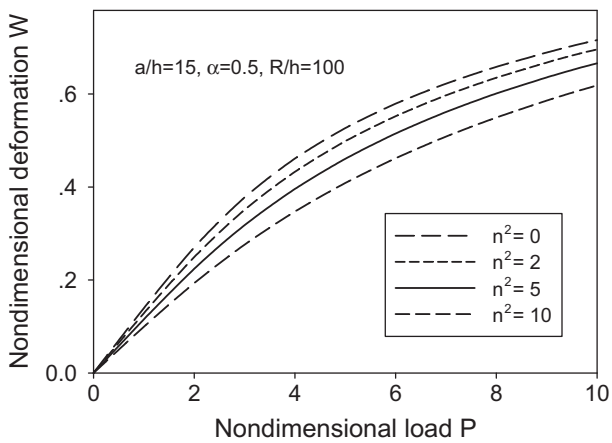

Fig. 11. Influence of residual stress on the center deflection for $a/h = 15$, $R/h = 100$ and $\alpha = 0.5$ in the case of small deflection.

The effects of the residual stress (n^2) on the contact radius and center deflection are shown, respectively, in Figs. 10 and 11 for fixed $a/h = 15$, $R/h = 100$ and $\alpha = 0.5$. It is demonstrated that the residual stress in the film can significantly affect the deflection of the blister. The larger the residual stress is, the smaller the contact radius (Fig. 10) and center deflection (Fig. 11) are.

5.2. Numerical solutions in the case of large deflection

In this subsection, an iteration approach is adopted to obtain the numerical solution of the blister test in the case of large deflection.

For the contact region, substituting Eq. (14) into Eq. (7c) gives the solution of the displacement in the radial direction

$$U_c = \frac{C_7}{x} + xC_8 + \frac{1}{8tx}\left\{\frac{2R^2}{a^2} + (\nu_f + 1)\frac{R^2}{a^2}\log(R^2 - a^2x^2) + x^2(\nu_f - 1)[1 - \log(R^2 - a^2x^2)]\right\}, \tag{28}$$

where the constants C_7 and C_8 are to be determined from the boundary and continuity conditions, and

$$U_c = u_c/h. \tag{29}$$

In the case of large deflection, substituting Eqs. (26a,b,c) and (28) into Eq. (25) gives

$$W_{c0} = W_n|_{x=x_0} + \frac{R}{h}\left[1 - \sqrt{1 - (\frac{x_0 a}{R})^2}\right], \tag{30a}$$

$$C_5 = -\frac{1}{I_1(bx_0)}\left[\frac{dW_n}{dx}\bigg|_{x=x_0} + \varphi_{c0}|_{x=x_0}\right], \tag{30b}$$

$$C_8 = \frac{t}{12(1-\nu_f^2)}\left[x_0\frac{d\Delta N_n}{dx}\bigg|_{x=x_0} + (1-\nu_f)\Delta N_n|_{x=x_0}\right] - \frac{1}{8x_0 t}\left\{x_0^2(\nu_f-1)[1-\log(R^2-a^2x_0^2)] + \frac{R^2}{a^2}(1+\nu_f)\log\left(\frac{R^2-a^2x_0^2}{R^2}\right)\right\}, \tag{30c}$$

$$\frac{x_0}{1-\nu_f}\frac{d\Delta N_n}{dx}\bigg|_{x=x_0} + \frac{6a^2x_0^2}{R^2-a^2x_0^2}\frac{a^2}{h^2} + \frac{3}{2t^3}\left[\frac{2a^2x_0^2(\nu_f-1)}{R^2-a^2x_0^2} - \frac{2R^2(\nu_f+1)}{R^2-a^2x_0^2} - 2(\nu_f+1)\frac{R^2}{a^2x_0^2}\log\left(\frac{R^2-a^2x_0^2}{R^2}\right)\right] = 0, \tag{30d}$$

$$\frac{d^3W_n}{dx^3}\bigg|_{x=x_0} + \frac{1}{x_0}\frac{d^2W_n}{dx^2}\bigg|_{x=x_0} - \frac{1}{x_0^2}\frac{dW_n}{dx}\bigg|_{x=x_0} - b^2\frac{dW_n}{dx}\bigg|_{x=x_0} = b^2\frac{x_0 a}{tR}\left[1-\left(\frac{x_0 a}{R}\right)^2\right]^{-\frac{1}{2}}, \tag{30e}$$

$$\frac{d^2W_n}{dx^2}\bigg|_{x=x_0} - \frac{[I_0(bx_0)+I_2(bx_0)]b}{2I_1(bx_0)}\frac{dW_n}{dx}\bigg|_{x=x_0} = \frac{d\varphi_{c0}}{dx}\bigg|_{x=x_0} - \frac{b\varphi_{c0}|_{x=x_0}}{2I_1(bx_0)}[I_0(bx_0)+I_2(bx_0)]. \tag{30f}$$

For a given contact radius x_0, the three continuity conditions in Eqs. (30d), (30e), and (30f) and the three boundary conditions in Eq. (23) along the blister edge constitute the boundary values of Eqs. (1) and (2). This boundary value problem can be solved by employing the shooting method.

If the initial conditions at the contact ring $x = x_0$ are assumed to be

$$\Delta N_n = \chi, \quad W_n = \varsigma, \quad \frac{d^2W_n}{dx^2} = \xi, \tag{31}$$

the solution to Eq. (1) and (2) subject to the conditions in Eq. (30d), (30e), and (30f) can be expressed as

$$\Delta N_n = \Delta N_n(x,\chi,\varsigma,\xi), \quad W_n = W_n(x,\chi,\varsigma,\xi), \quad \frac{d^2W_n}{dx^2} = \frac{d^2W_n}{dx^2}(x,\chi,\varsigma,\xi), \tag{32}$$

which must satisfy the boundary conditions given in Eq. (23):

$$\begin{aligned} f_1(\chi,\varsigma,\xi) &\equiv \frac{1}{(1-\nu_f^2)t}\left[\frac{d\Delta N_n}{dx}\bigg|_{x=1} + (1-\nu_f)\Delta N_n|_{x=1}\right] + C_{NN}\Delta N_n|_{x=1} + C_{NQ}tk_1 + C_{NM}k_2, \\ f_2(\chi,\varsigma,\xi) &\equiv \frac{12}{t^2}W_n|_{x=1} + C_{NQ}\Delta N_n|_{x=1} + C_{QQ}tk_1 + C_{QM}k_2, \\ f_3(\chi,\varsigma,\xi) &\equiv \frac{12}{t}\frac{dW_n}{dx}\bigg|_{x=1} + C_{NM}\Delta N_n|_{x=1} + C_{QM}tk_1 + C_{MM}k_2, \end{aligned} \tag{33}$$

where

$$\begin{aligned} k_1 &= \Delta N_n|_{x=1}\frac{dW_n}{dx}\bigg|_{x=1} - \frac{d^3W_n}{dx^3}\bigg|_{x=1} - \frac{d^2W_n}{dx^2}\bigg|_{x=1} + \frac{dW_n}{dx}\bigg|_{x=1}, \\ k_2 &= \frac{d^2W_n}{dx^2}\bigg|_{x=1} + \nu_f\frac{dW_n}{dx}\bigg|_{x=1}. \end{aligned} \tag{34}$$

The values of χ, ζ and ξ are determined using the Newton–Raphson iterative approach:

$$\begin{bmatrix}\chi^{k+1}\\ \varsigma^{k+1}\\ \xi^{k+1}\end{bmatrix} = \begin{bmatrix}\chi^{k}\\ \varsigma^{k}\\ \xi^{k}\end{bmatrix} + \begin{bmatrix}\delta\chi^{k+1}\\ \delta\varsigma^{k+1}\\ \delta\xi^{k+1}\end{bmatrix}, \tag{35a}$$

$$\begin{bmatrix}\frac{\partial f_1}{\partial\chi} & \frac{\partial f_1}{\partial\varsigma} & \frac{\partial f_1}{\partial\xi}\\ \frac{\partial f_2}{\partial\chi} & \frac{\partial f_2}{\partial\varsigma} & \frac{\partial f_2}{\partial\xi}\\ \frac{\partial f_3}{\partial\chi} & \frac{\partial f_3}{\partial\varsigma} & \frac{\partial f_3}{\partial\xi}\end{bmatrix}\begin{bmatrix}\delta\chi^{k+1}\\ \delta\varsigma^{k+1}\\ \delta\xi^{k+1}\end{bmatrix} = -\begin{bmatrix}f_1^{k+1}\\ f_2^{k+1}\\ f_3^{k+1}\end{bmatrix}, \tag{35b}$$

whereby the solution is found when a preset accuracy criterion is satisfied: i.e.,

$$|f_1^{(n)}| + |f_2^{(n)}| + |f_3^{(n)}| < \Delta, \tag{36}$$

where Δ is a small positive quantity. In the present paper, we take $\Delta = 10^{-6}$. The functions $f_1(\chi,\varsigma,\xi)$, $f_2(\chi,\varsigma,\xi)$ and $f_3(\chi,\varsigma,\xi)$ cannot be expressed explicitly, and thus, all calculations are numerical.

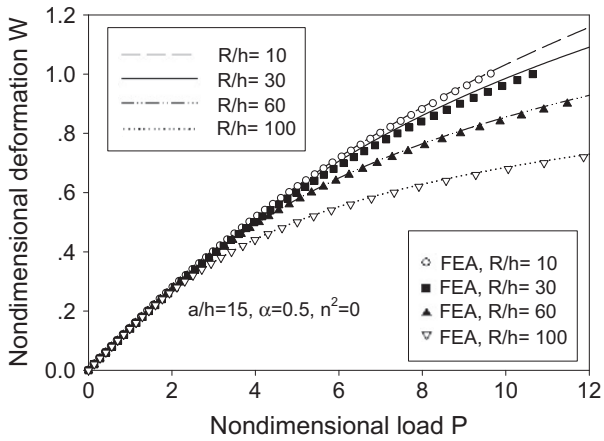

Fig. 12. Comparison of the center deflections based on the numerical solution and FEA for different indenter radii in the case of large deflection.

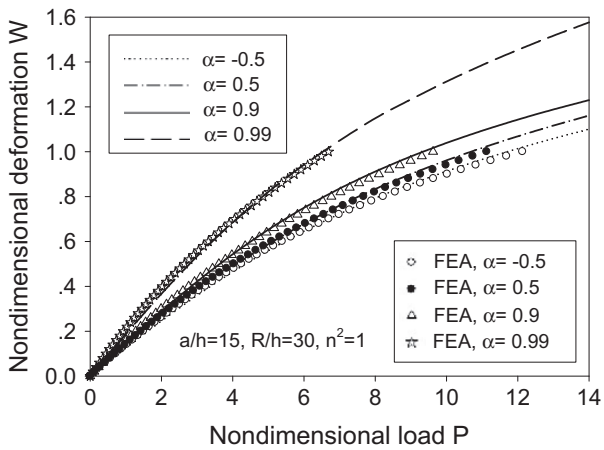

Fig. 13. Comparison of the center deflections based on the numerical solution and FEA for different values of Dundur's parameter in the case of large deflection.

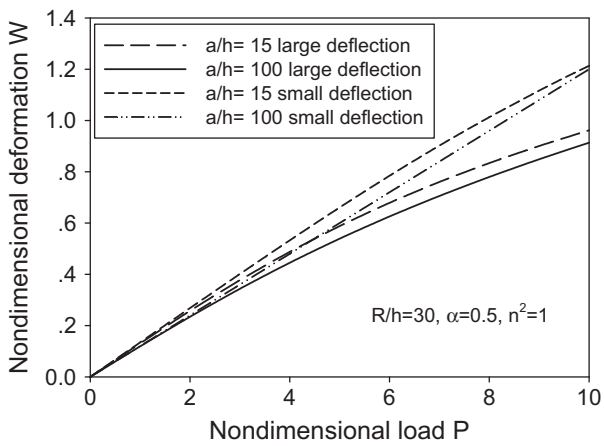

Fig. 14. Comparison of the center deflections based on small deflection and large deflection theories for different blister sizes.

Based on the solution obtained above, a new value of x_0 is determined using the equilibrium equation at $x = x_0$:

$$\Delta N_{\mathrm{n}}\big|_{x=x_0}\frac{dW_{\mathrm{n}}}{dx}\bigg|_{x=x_0}-\frac{d^3W_{\mathrm{n}}}{dx^3}\bigg|_{x=x_0}-\frac{1}{x_0}\frac{d^2W_{\mathrm{n}}}{dx^2}\bigg|_{x=x_0}+\frac{1}{x_0^2}\frac{dW_{\mathrm{n}}}{dx}\bigg|_{x=x_0}=-\frac{P}{x_0}. \tag{37}$$

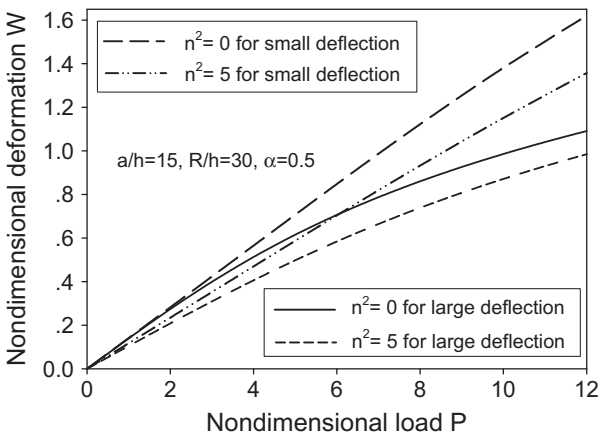

Fig. 15. Comparison of the center deflections based on small-deflection and large-deflection theories for different residual stresses.

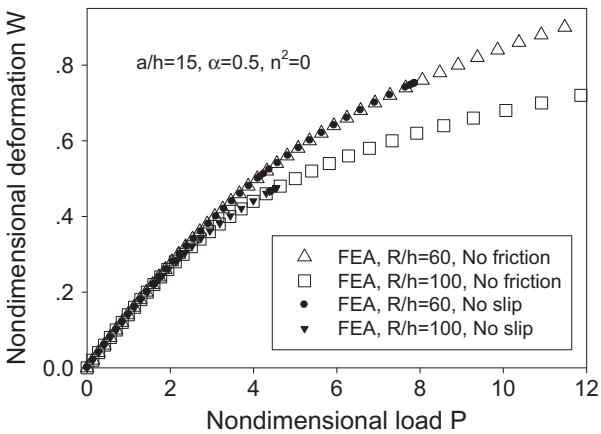

Fig. 16. Influence of friction on the center deflections based on the large-deflection theory obtained using the finite-element method.

Thus, one iteration has been completed. The iteration procedure continues until the equilibrium equation is satisfied.

Fig. 12 shows the deflection at the blister center obtained by employing the proposed iteration approach as compared to that from FEA. Other fixed parameters are $a/h = 15$, $\alpha = 0.5$ and $n^2 = 0$. It is seen that the result from the iteration approach compare favorably to that of the FEA. It is further observed that the larger the indenter radius is, the smaller the film deflection is.

Fig. 13 plots the normalized deflection W versus the normalized load P for different Dundur's parameter based on both the iteration approach and the FEA. It is clear that the substrate deformation has great influence on the blister deflection especially when a stiff film is on a soft substrate.

Figs. 14 and 15 show the normalized blister deflection versus the normalized load based on both the small-deflection and large-deflection theories. The results demonstrate that when the load is relatively large (e.g., $P > 4$), the large-deflection theory must be employed to predict the deflection–load curve.

6. Influence of the friction between the indenter and film

It is well known that there is friction between the indenter and film. In the solutions obtained in the last section, the friction is assumed to be zero. The influence of friction is studied by employing the FEA. Fig. 16 plots the deflection versus load with zero friction and infinite friction (i.e., no slip). These correspond to the lower and upper bounds of the friction. The results show that, for a relatively small load, the influence of the friction is negligible. For example, for $R/h = 60$ and $P = 7.65$, the normalized deflection is $W = 0.7400$ and $W = 0.7406$, respectively, for the zero- and infinite-friction cases.

7. Concluding remarks

Comprehensive mechanics for the spherically capped shaft- or ball-loaded blister test methods is developed where the Reissner's plate bending theory is employed to depict the deflection of the thin film in the contact region. The analytical solution for small deflection and the numerical (iteration) solution for large deflection are developed. These solutions take into

account the effect of the ball or spherical cap radius, the substrate deformation, the residual stress, and the elastic mismatch between the film and substrate. Numerical results show that these parameters could significantly influence the relation between the blister center deflection and applied load. Both the analytical and iteration solutions were verified by FEA. It is interesting to point out that, even in the case of small deflection, the deflection–load relation is nonlinear owing to the contact between the film and loading ball or loading spherical cap. The developed mechanics should be very useful to blister tests where the elastic modulus, residual stress in the film, and interface fracture toughness between the film and substrate can be determined.

Acknowledgements

The work was supported by the National Natural Science Foundation of China (No. 10872184) and the Innovation Scientists and Technicians Troop Construction Projects of Henan Province (No. 084200510004) and Program for Innovative Research Team (in Science and Technology) in University of Henan Province (No. 2010IRTSTHN013).

Appendix A. Particular solution to Eq. (11)

It is difficult to obtain an exact analytical solution for Eq. (11). However, using the Taylor series

$$\frac{\partial w_c}{\partial r} = -\frac{r}{R} - \frac{r^3}{2R^3} - \frac{3r^5}{8R^5} - \frac{5r^7}{16R^7} - \cdots, \tag{A1}$$

we can obtain a solution in the series form. Thus, an approximate analytical solution can be obtained using a truncated Taylor series. For instance, when $k = 4$ (i.e., only the first two terms are used), the error of $\frac{\partial w_c}{\partial r}$ is less than 0.2% for $r/R \leqslant 0.5$. Therefore, Eq. (11) can be reduced to

$$\frac{\partial^2 \varphi_c}{\partial x^2} + \frac{1}{x}\frac{\partial \varphi_c}{\partial x} - \left(\frac{1}{x^2} + \frac{Ca^2}{D}\right)\varphi_c = \frac{Ca^2}{D}\frac{a}{h}\left(\frac{xa}{R} + \frac{x^3a^3}{2R^3}\right). \tag{A2}$$

Thus, the particular solution φ_{c0} of Eq. (A2) can be expressed as

$$\begin{aligned}\varphi_{c0} = &-\tfrac{ia^2\pi x^3}{8hR^3}\big[8a^2 I_3(bx)Y_1(-ibx) + 2a^2 bx I_4(bx)Y_1(-ibx)\\ &+b^3R^2xY_1(-ibx)\tfrac{{}_0F_1(3,b^2x^2/4)}{\Gamma(3)}\\ &-ia^2b^2x^2J_1(-ibx)G_M[\{\{-\tfrac{2}{3}\},\{-1\},\{\{-\tfrac{1}{2},\tfrac{1}{2}\},\{-\tfrac{5}{2},-1\}\},-\tfrac{1}{2}ibx,\tfrac{1}{2}]\\ &-2ib^2R^2J_1(-ibx)G_M[\{\{-\tfrac{1}{2}\},\{-1\},\{\{-\tfrac{1}{2},\tfrac{1}{2}\},\{-\tfrac{3}{2},-1\}\},-\tfrac{1}{2}ibx,\tfrac{1}{2}]\big],\end{aligned} \tag{A3}$$

where G_M is the Meijer G function, $\Gamma(x)$ is the Gamma function, $J_m(x)$ and $Y_m(x)$ are, respectively, the first- and second-kind Bessel functions of mth order, and ${}_0F_1(3, b^2x^2/4)$ is the confluent hypergeometric function

$${}_0F_1(\delta, x) = \sum_{j=0}^{\infty} \frac{1}{(\delta)_j}\frac{(x)^j}{j!}. \tag{A14}$$

In this paper, we set $k = 4$ for small deflection and $k = 8$ for large deflection.

Appendix B. Coefficients in the final solution of Eq. (26).

The coefficients in the final solution of Eq. (26) are

$$C_3 = \frac{C_{3a}}{C_{3b}}, \tag{B1}$$

$$C_2 = \frac{P + L_1C_3}{L_2}, \tag{B2}$$

$$C_1 = \frac{1}{d_6 - 1}(C_2L_3 + C_3L_4), \tag{B3}$$

$$C_4 = C_1d_1 + C_2\left[\frac{1}{n^2} - d_2I_0(n) + d_3I_1(n) + d_4I_2(n) + d_5I_3(n)\right] - C_3[d_2K_0(n) + d_3K_1(n) - d_4K_2(n) + d_5K_3(n)], \tag{B4}$$

$$C_5 = [-\varphi_{c0}|_{x=x_0} + \frac{C_1}{x_0} + \frac{I_1(nx_0)}{n}C_2 - \frac{K_1(nx_0)}{n}C_3]/I_1(bx_0), \tag{B5}$$

$$C_6 = 0, \tag{B6}$$

$$C_7 = -\frac{1}{8t}\frac{R^2}{a^2}[2 + (1+\nu_f)\log R^2], \tag{B7}$$

where $I_m(x)$ and $K_m(x)$ are, respectively, the first- and second-kind modified Bessel functions of the mth order, and

$$\begin{aligned} C_{3a} &= \frac{a^2 x_0}{hR\sqrt{1-(x_0 a/R)^2}} + \left[\frac{L_3}{x_0(d_6-1)} + \frac{I_1(nx_0)}{n} - \frac{L_5}{b^2}\right]\frac{P}{L_2}, \\ C_{3b} &= \frac{1}{b^2}\left[\frac{L_5 L_1}{L_2} + L_6\right] - \frac{1}{x_0(d_6-1)}\left[\frac{L_1 L_3}{L_2} + L_4\right] - \frac{I_1(nx_0)}{n}\frac{L_1}{L_2} + \frac{K_1(nx_0)}{n}, \end{aligned} \tag{B8}$$

$$\begin{aligned} d_1 &= \frac{1}{12}t^2(1-\nu_f)C_{QM}, \\ d_2 &= \frac{1}{n^2} + \frac{1}{24}(t^2 C_{QM} - t^3 C_{QQ}), \\ d_3 &= \left(\frac{3}{4}n - \frac{1}{n}\right)\frac{1}{12}t^3 C_{QQ} - \frac{1}{12n}t^2 C_{QM}\nu_f, \\ d_4 &= \frac{1}{24}(t^3 C_{QQ} - t^2 C_{QM}), \\ d_5 &= \frac{1}{48}nt^3 C_{QQ}, \\ d_6 &= \frac{1}{12}t(1-\nu_f)C_{MM}, \\ d_7 &= \frac{1}{24}(tC_{MM} - t^2 C_{QM}), \\ d_8 &= \frac{1}{n} - \left(\frac{3}{4}n - \frac{1}{n}\right)\frac{1}{12}t^2 C_{QM} + \frac{1}{12n}tC_{MM}\nu_f, \\ d_9 &= \frac{1}{48}nt^2 C_{QM}, \end{aligned} \tag{B9}$$

$$\begin{aligned} L_1 &= \frac{3}{4}nK_1(n) + \frac{1}{4}nK_3(n) - \frac{1}{2}K_0(n) - \frac{1}{2}K_2(n) - \frac{1}{n}K_1(n), \\ L_2 &= \frac{3}{4}nI_1(n) + \frac{1}{4}nI_3(n) + \frac{1}{2}I_0(n) + \frac{1}{2}I_2(n) - \frac{1}{n}I_1(n), \\ L_3 &= d_7 I_0(n) + d_8 I_1(n) + d_7 I_2(n) - d_9 I_3(n), \\ L_4 &= d_7 K_0(n) - d_8 K_1(n) + d_7 K_2(n) + d_9 K_3(n), \\ L_5 &= \frac{1}{2x_0}I_0(nx_0) + \left(\frac{3}{4}n - \frac{1}{nx_0^2}\right)I_1(nx_0) + \frac{1}{2x_0}I_2(nx_0) + \frac{1}{4}nI_3(nx_0), \\ L_6 &= \frac{1}{2x_0}K_0(nx_0) - \left(\frac{3}{4}n - \frac{1}{nx_0^2}\right)K_1(nx_0) + \frac{1}{2x_0}K_2(nx_0) - \frac{1}{4}nK_3(nx_0). \end{aligned} \tag{B10}$$

Reference

Allen, M. G., & Senturia, S. D. (1989). Application of the island blister test for thin film adhesion measurement. *Journal of Adhesion, 29*, 219–231.

Antunes, J. M., Fernandes, J. V., Sakharova, N. A., Oliveira, M. C., & Menezes, L. F. (2007). On the determination of the Young's modulus of thin films using indentation test. *International Journal of Solids and Structures, 44*, 8313–8334.

Arjun, A., & Wan, K. T. (2005). Derivation of the strain energy release rate G from first principles for the pressurized blister test. *International Journal of Adhesion and Adhesives, 25*, 13–18.

Bennett, S. J., Devries, K. L., & Williams, M. L. (1974). Adhesive fracture mechanics. *International Journal of Fracture, 10*, 33–43.

Chang, W. V., & Peng, S. H. (1992). Nonlinear elastic analysis of adhesive blister test. *International Journal of Fracture, 53*, 77–89.

Dannenberg, H. (1961). Measurement of adhesion by a blister method. *Journal of Applied Polymer Science, 5*, 125–134.

Dillard, D. A., & Bao, Y. (1991). The peninsula blister test: a high and constant strain energy release rate fracture specimen for adhesives. *Journal of Adhesion, 33*, 253–271.

Fernando, M., & Kinloch, A. J. (1990). Use of the 'inverted-blister' test to study the adhesion of photopolymers. *International Journal of Adhesion and Adhesives, 10*, 69–76.

Gent, A. N., & Hamed, G. R. (1977). Peel mechanics for an elastic–plastic adherend. *Journal of Applied Polymer Science, 21*, 2817–2831.

Gecit, M. R. (1987). Pull-off test for a cracked layer bonded to a rigid foundation. *International Journal of Engineering Science, 25*, 807–820.

Hbaieb, K., & Zhang, Y. W. (2005). A parametric study of a pressurized blister test for an elastic–plastic film-rigid substrate system. *Materials Science and Engineering A, 390*, 385–392.

Hinkley, J. A. (1983). A blister test for adhesion of polymer films to SiO_2. *Journal of Adhesion, 16*, 115–126.

Hohlfelder, R. J., Luo, H., Vlasska, J. J., Chidsey, C. E. D., & Nix, W. D. (1997). Measuring interfacial fracture toughness with the blister test. *Materials Research Society Symposium Proceedings, 436*, 115–120.

Jensen, H. M. (1991). The blister test for interface toughness measurement. *Engineering Fracture Mechanics, 40*, 475–486.

Jensen, H. M., & Thouness, M. D. (1993). Effects of residual stresses in the blister test. *International Journal of Solids and Structures, 30*, 779–795.
Jiang, L. M., Zhou, Y. C., Liao, Y. G., & Sun, C. Q. (2008). A pressurized blister test model for the interface adhesion of dissimilar elastic–plastic materials. *Materials Science and Engineering A, 487*, 228–234.
Jin, C. (2008). Analysis of energy release rate and bending-to-stretching behavior in the shaft-loaded blister test. *International Journal of Solids and Structures, 45*, 6485–6500.
Jin, C., & Wang, X. D. (2008). A theoretical study of a thin-film delamination using shaft-loaded blister test: Constitutive relation without delamination. *Journal of the Mechanics and Physics of Solids, 56*, 2815–2831.
Johnson, K. L. (1985). *Contact mechanics*. Cambridge University Press.
Kahrobaiyan, M. H., Asghari, M., Rahaeifard, M., & Ahmadian, M. T. (2010). Investigation of the size-dependent dynamic characteristics of atomic force microscope microcantilevers based on the modified couple stress theory. *International Journal of Engineering Science, 48*, 1985–1994.
Khan, M. B. (1995). Biaxial stretching analysis for simulation of composite fracture using blister test. *Composites, 26*, 223–227.
Kozlova, O., Braccini, M., Eustathopoulos, N., Devismes, M. F., & Dupeux, M. (2008). Shaft loaded blister test for metal/ceramic brazing fracture. *Materials Letters, 62*, 3626–3628.
Lai, Y. H., & Dillard, D. (1994). A study of the fracture efficiency parameter of blister tests for films and coatings. *Journal of Adhesion Science and Technology, 8*, 663–678.
Lee, C. C., Huang, J., Chang, S. T., & Wang, W. C. (2009). Adhesion investigation of low-k films system using 4-point bending test. *Thin Solid Films, 517*, 4875–4878.
Lee, D. H., Barber, J. R., & Thouless, M. D. (2009). Indentation of an elastic half space with material properties varying with depth. *International Journal of Engineering Science, 47*, 1274–1283.
Li, J. K., & Chou, T. W. (1997). Elastic field of a thin-film/substrate system under an axisymmetric loading. *International Journal of Solids and Structures, 34*, 4463–4478.
Liao, K., & Wan, K. T. (2000). Delamination behavior of film–substrate systems under cyclic loading. *Journal of Materials Science Letters, 19*, 57–59.
Ma, L. S., & Wang, T. J. (2004). Relationships between axisymmetric bending and buckling solutions of FGM circular plates based on third-order plate theory and classical plate theory. *International Journal of Solids and Structures, 41*, 85–101.
Malyshev, B. M., & Salganik, R. L. (1965). The strength of adhesive joints using the theory of cracks. *International Journal of Fracture Mechanics, 1*, 114–128.
O'Brien, E. P., Ward, T. C., Guo, S., & Dillard, D. A. (2003). Strain energy release rates of a pressure sensitive adhesive measured by the shaft-loaded blister test. *Journal of Adhesion, 79*, 69–97.
Perry, A. J. (1983). Scratch adhesion testing of hard coatings. *Thin Solid Films, 107*, 167–180.
Pharr, C. M., & Oliver, W. C. (1992). Measurement of thin film mechanical properties using nanoindentation. *MRS Bulletin, 17*, 34–45.
Reddy, J. N., & Wang, C. M. (2000). An overview of the relationships between solutions of the classical and shear deformation plate theories. *Composites Science and Technology, 60*, 2327–2335.
Sizemore, J., Hohlfelder, R. J., Vlassak, J. J., & Nix, W. D. (1995). Measuring the adhesion of diamond thin films to substrates using the blister test. *Materials Research Society Symposium Proceedings, 383*, 197–207.
Small, M. K., & Nix, W. D. (1992). Analysis of the accuracy of the bulge test in determining the mechanical properties of thin films. *Journal of Materials Research, 7*, 1553–1563.
Timoshenko, S. (1957). *Strength of materials, Part II, Advanced theory and problems* (3rd ed.). New York: Van Nostrand Company.
Timoshenko, S., & Woinowsky-Krieger, S. (1959). *Theory of plates and shells. Engineering societies monographs* (2nd ed). New York: McGraw-Hill.
Volinsky, A. A., Moody, N. R., & Gerberich, W. W. (2002). Interfacial toughness measurements for thin films on substrates. *Acta Materialia, 50*, 441–466.
Voorthuyzen, J. A., & Bergveld, P. (1984). The influence of tensile forces on the deflection of circular diaphragms in pressure sensors. *Sensors and Actuators, 6*, 201–213.
Wan, K. T. (1999). Fracture mechanics of a shaft-loaded blister test-transition from a bending plate to a stretching membrane. *Journal of Adhesion, 70*, 209–219.
Wan, K. T., Guo, S., & Dillard, D. (2003). A theoretical and numerical study of a thin clamped circular film under an external load in the presence of residual stress. *Thin Solid Films, 425*, 150–162.
Wan, K. T., & Liao, K. (1999). Measuring mechanical properties of thin flexible film by a shaft-loaded blister test. *Thin Solid Films, 352*, 167–172.
Wan, K. T., & Mai, Y. W. (1995). Fracture mechanics of a shaft-loaded blister of thin flexible membrane on rigid substrate. *International Journal of Fracture, 74*, 181–197.
Weihs, T. P., Hong, S., Bravman, J. C., & Nix, W. D. (1988). Mechanical deflection of cantilever microbeams: A new technique for testing the mechanical properties of thin films. *Journal of Materials Research, 3*, 931–942.
Williams, M. L. (1969). The continuum interpretation for fracture and adhesion. *Journal of Applied Polymer Science, 13*, 29–40.
Xu, X. J., Shearwood, C., & Liao, K. (2003). A shaft-loaded blister test for elastic response and delamination behavior of thin film–substrate system. *Thin Solid Films, 424*, 115–119.
Zhang, T.-Y., Su, Y. J., Qian, C. F., Zhao, M. H., & Chen, L. Q. (2000). Microbridge testing of silicon nitride thin films deposited on silicon wafers. *Acta Materialia, 48*, 2843–2857.
Zhao, M. H., Zhang, K., & Zhang, T.-Y. (2010). Reissner plate-theory-based study of circular and annular delamination buckling of a film on a substrate. *Engineering Fracture Mechanics, 77*, 1479–1491.
Zhao, M. H., Zheng, W. L., & Fan, C. Y. (2010). Mechanics of shaft-loaded blister test for thin film suspended on compliant substrate. *International Journal of Solids and Structures, 47*, 2525–2532.
Zhao, M. H., Zhou, J., Yang, F., Liu, T., & Zhang, T.-Y. (2007). Effects of substrate compliance on circular buckle delamination of thin films. *Engineering Fracture Mechanics, 74*, 2334–2351.